

MATERIALS SCIENCE

Surface slip on rotating graphene membrane enables the temporal selectivity that breaks the permeability-selectivity trade-off

Zhongqiang Zhang^{1,2,3*}, Shaofan Li^{1*†}, Baoxia Mi¹, Jinbao Wang⁴, Jianning Ding^{2,3†}

Membrane separation technology is dictated by the permeability-selectivity trade-off rule, because selectivity relies on membrane pore size being smaller than that of hydrated ions. We discovered a previously unknown mechanism that breaks the permeability-selectivity trade-off in using a rotating nanoporous graphene membrane with pores of 2 to 4 nanometers in diameter. The results show that the rotating membrane exhibits almost 100% salt rejection even when the pore size is larger than that of hydrated ions, and the surface slip at the liquid/graphene interface of rotating membrane enables concurrent ultra-selectivity and unprecedented high permeability. A novel concept of “temporal selectivity” is proposed to attribute the unconventional selectivity to the time difference between the ion’s penetration time through the pore and the bypass time required for ion’s sliding across the pore. The newly discovered temporal selectivity overcomes the limitation imposed by pore size and provokes a novel theory in designing high-performance membranes.

INTRODUCTION

Fresh water is one of the most precious resources for the survival of human beings and other lives, but its availability is getting more and more strained because of population growth, climate change, and water pollution. Despite the abundance of seawater as an alternative water resource, seawater desalination is usually limited by relatively low productivity and high energy consumption. Membrane-based desalination technologies including the state-of-the-art reverse osmosis (RO) technology have been demonstrated to be more energy efficient than thermal desalination approaches (1, 2). However, conventional polymeric RO membranes still suffer deficiencies such as low fouling resistance, poor selectivity, and low stability to resist chemical/heat-induced degradation. Therefore, it has been an ever-continuous endeavor to search and explore new materials for fabricating membranes with improved permeability, selectivity, chemical stability, and resistance to fouling simultaneously (3). Three types of novel membranes have demonstrated great promises in addressing water permeability and selectivity. They are ultrathin nanoporous membranes, e.g., porous graphene (4–11), membranes with artificial water channels such as carbon nanotubes (CNTs) (12–19), and layer-stacked membranes with two-dimensional water channels, including graphene oxide (GO) (20–24) and MoS₂ (25, 26).

Theoretically, a membrane with atomic thickness can lead to a water permeance two to three orders of magnitude higher than that of conventional membranes due to the inversely proportional relationship between water flux and membrane thickness (2, 4). Thus, the atomic thickness of nanoporous graphene (~0.34 nm) may result in larger water permeability (6 to 66 liter/cm² per day per MPa) than thin-film composite (TFC) membranes (~0.24 liter/cm² per day per

MPa) (27) while achieving a complete salt rejection (100%). It has been demonstrated by both the molecular dynamics (MD) simulations (4) and experiments (9). In addition, graphene materials exhibit fouling resistance, resistance to degradation (28), ultrahigh mechanical strength for preventing ripping, tunable small pore size for controllable permeability, chemical stability, and scalable synthesis method that may lead to cost-effective production. Because of these advantages, graphene-based membranes are identified as promising candidates for next-generation seawater desalination systems. However, the use of nanoporous graphene is still a work in progress for seawater desalination due to the difficulties in drilling defect-free subnanometer pores with uniform radius of <0.45 nm on a monolayer graphene (29). A primary reason for this is the requirement of uniform subnanoscale-sized pore distribution, which determines the selectivity of nanoporous graphene, posing a serious challenge in fabrication of the nanoporous membranes. This is the key factor that has been hindering the large-scale applications of porous graphene-based membrane technology.

CNTs are another class of materials that have great potential for RO desalination, which was first demonstrated by MD simulations (12). A single-walled (6,6) CNT with the diameter of 0.81 nm can reject salt completely and generate high water permeability of 14.33 liter/cm² per day per MPa attributed to its smooth and non-polar interior. However, the salt rejection decreases sharply to 58% when the CNT diameter increases to 1.1 nm. Subsequently, aligned CNT-based membranes were fabricated experimentally by chemical vapor deposition methods (14, 15). The experimental results indicate that the water flux is three to five orders of magnitude higher than that predicted by continuum theory. Unfortunately, however, the fabricated CNT-based membranes with the CNT diameter ranging from 1.6 to 7 nm and above cannot reject the sub-2-nm particles, indicating that they are not suitable for seawater desalination at current stage unless the uniform single-walled (6,6) CNTs can be well dispersed and aligned in the membrane in the future.

Other types of nanomaterial membranes have been developed. For instance, the interlayer spacing of GO membrane can be controlled in the range of 0.64 to 0.98 nm to realize 97% rejection for NaCl

¹Department of Civil and Environmental Engineering, University of California, Berkeley, Berkeley, CA 94720-1710, USA. ²Institute of Intelligent Flexible Mechatronics, Jiangsu University, Zhenjiang 212013, P.R. China. ³Jiangsu Collaborative Innovation Center of Photovoltaic Science and Engineering, Changzhou University, Changzhou 213164, P.R. China. ⁴School of Naval Architecture and Civil Engineering, Zhejiang Ocean University, Zhoushan 316000, P.R. China.

*These authors contributed equally to this work.

†Corresponding author. Email: shaofan@berkeley.edu (S.L.); dingjn@ujs.edu.cn (J.D.)

(24). Fully hydrated MoS₂ membranes with free spacing of 0.9 nm exhibit high water permeability up to 6 liter/cm² per day per MPa and moderate-to-high ionic rejection of 90% (25). Recently, a large area graphene-nanomesh/CNT hybrid membrane with average pore size of 0.63 nm is fabricated experimentally to realize water permeability of 2.4 liter/cm² per day per MPa with a stable salt rejection of 86% (30). The high salt rejection efficiency of 93 to 100% for a large pore size of 1.44 nm in diameter has been demonstrated for charged monolayer nanoporous graphene membranes, while the required pressure drop is reduced substantially (31, 32). To break the limitation of porous graphene for molecular sieving, both the ion-gated and charged porous graphene membrane models have been proposed to tune nonselective larger pores of 0.52 to 0.6 nm to be selective for gas separation (33, 34).

In summary, up to date, none of the novel membrane materials that have been explored in the literature is able to break the trade-off rule between permeability and selectivity. Although nanoporous monolayer graphene and CNT-based membranes are of high permeability because of their ultrathin thickness and fast water diffusion property, the fabrication of uniform subnanometer pores on a graphene sheet or the fabrication of uniformly dispersed small-diameter CNTs to form an assembled membrane presents great technical difficulties and challenges. The ultimate contradiction of selectively permeable membrane technology is that the size of nanopores should be smaller than the diameter of hydrated ions to exhibit enhanced ion selectivity while hoping for high permeability, which is a paradoxical issue or a trade-off that was thought as an insurmountable obstacle. In this study, we report a novel concept of desalination mechanism of temporal selectivity using slip-induced separation that breaks the permeability-selectivity trade-off without stringently relying on small, uniform pore sizes. The desalination is achieved by rotating porous monolayer graphene cylinder (GC) with large pores that are two to five times larger than the diameter of hydrated sodium ions (Fig. 1). The boundary slip at the water-GC interface significantly enhances the salt rejection. At the same time, the large nanopores results in an ultrahigh water flux under centrifuge-induced pressure. Therefore, this novel slip-induced separation bypasses the conventional limitation of pore size and breaks the trade-off between permeability and selectivity. Moreover, the required permeability and selectivity can be obtained by adjusting the porosity, the pore size, the thickness of membrane, and the rotating velocity of porous hydrophobic membranes. The findings reported in this work may open a new door of designing highly efficient RO desalination apparatus, triggering a boom of both theoretical and experimental researches on rotating/shearing membranes, which may further revolutionize the design of the next-generation desalination and water purification technologies.

RESULTS

Permeability and selectivity are key indicators to assess the performances of RO membranes. Figure 2 (A and B) shows the relations between the numbers of both the penetrated water molecules and ions (sodium and chlorine) and time for different rotating angular velocities of the porous GC with 12 pores (porosity of 2.163%) of 2 nm in diameter. The penetrated water molecules increase approximately linearly with time despite some fluctuations caused by dynamic effects of the centrifuge rotation and the pressure release in penetrating process within the feed solution. Excitingly, we dis-

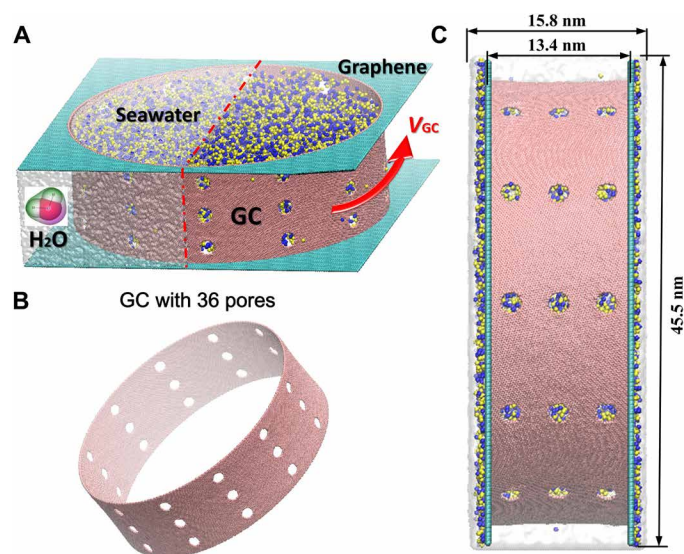


Fig. 1. Schematic illustration of the large-scale MD desalination model. (A) A nanoporous rotating GC (red) of 36 pores with a diameter of 2 nm, seawater (sodium ions in blue, chlorine ions in yellow, and transparent water molecules in the left half) confined in GC, pure water out of GC (transparent), and two porous graphene sheets (blue) to confine the draw solution. The diameter of the pore on graphene sheets is identical to that of GC. The red arrow denotes the rotating velocity of GC, V_{GC} . (B) Three-dimensional view of porous GC with 36 nanopores of 2 nm in diameter. (C) Dimension and relative position of each component. The feed solution is seawater confined within GC, and the draw solution is pure water confined by the outer surface of GC and two graphene sheets. The details of MD desalination model can be found in section S1. The movie of a representative graphene centrifuge with 36 pores rotating at angular velocity of 35 rad/ns is provided in movie S1.

covered that as the rotating angular velocity of porous membrane increases, less and less salt ions come out the porous GC, prevented by the rotating porous membrane, while more water molecules pass through the membrane. As shown in Fig. 2C, the salinity of feed solution can be reduced by two orders of magnitude from 3.5 to 0.059% for porous GC with 2-nm-diameter pores at the angular velocity of 40 rad/ns. Subsequently, we can find the freshwater flux and salt rejection as functions of the angular velocity of rotating porous GC, as illustrated in Fig. 2D. Here, the salt rejection is defined as $(1 - C_p/C_f) \times 100\%$, where C_p and C_f are the salt concentrations of permeated and feed solutions, respectively. It is found that both the salt rejection (selectivity) and water flux (permeability) concurrently increase with increasing the rotation speed of porous membrane. The rotating porous graphene with 2-nm-diameter nanopores exhibits a super salt rejection of 98.5% and an ultrahigh water flux of more than 3000 liter/cm² per day. The same conclusion can also be drawn from the MD results obtained under different porosities of 24 to 72 pores (see figs. S2 to S4). In other words, the trade-off between water permeability and selectivity can be completely broken by increasing the rotating angular velocity of the porous membranes even with such large nanopores. Moreover, no concentration polarization can be observed from the radial concentration distribution and radial density distributions of water molecules and ions obtained in the MD simulations (see section S5: fig. S5).

Nevertheless, it is noted that the pressure within the feed solution depends on the angular velocity due to the centrifugal force,

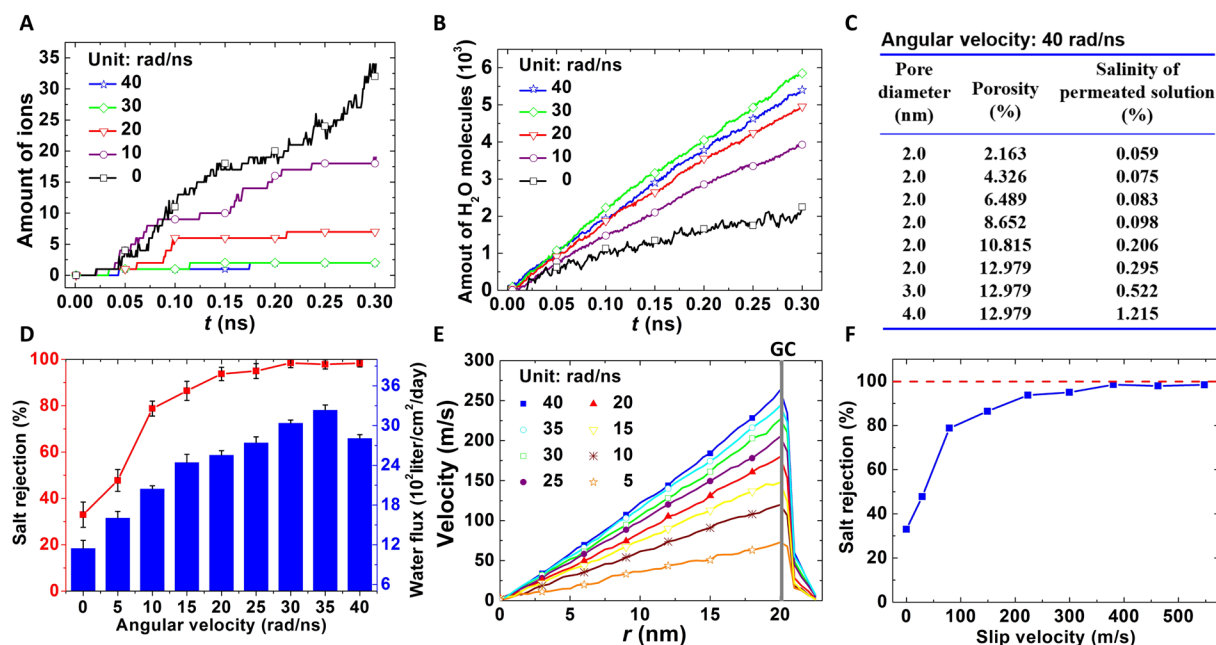


Fig. 2. Water flux and salt rejection influenced by angular velocity of GC. (A and B) Amounts of penetrated ions and water molecules versus time at angular velocity of 0, 10, 20, 30, and 40 rad/ns for the porous GC of 12 pores with 2 nm in diameter. (C) Salinity of filtered solutions for rotating GCs with different diameters of pores (2 to 4 nm) and porosities (the number of pores in range of 12 to 72 pores) at an angular velocity of 40 rad/ns. (D) Salt rejection and water flux as functions of angular velocity (0 to 40 rad/ns) for the porous GC with 12 2-nm-diameter pores. (E) Velocity profiles of the confined seawater for different angular velocities (5 to 40 rad/ns). The gray solid line denotes the radial position of porous GC. (F) Salt rejection as function of boundary slip velocity, i.e., velocity difference between the GC and boundary layer of seawater.

whereas the water permeability is usually characterized by a pressure-independent water flux in RO process. Because of the ultralow friction force between the hydrated molecules and the hydrophobic graphene surface (35), seawater will have large boundary slip on graphene surface (36). The feed pressure at feed seawater-membrane interface may be calculated by $P_{\text{feed}} = \frac{1}{2} \rho R^2 (\omega_{\text{GC}} - \omega_s)^2$ (see section S6), where ρ is the density of feed seawater, R is the radius of porous GC, ω_{GC} is the angular velocity of GC, and ω_s is the boundary slip angular velocity, i.e., v_s/R , where v_s is the boundary slip velocity, which can be obtained from the measured tangential velocity profiles (Fig. 2E). The magnitude of ion slip length found in this work is in the range of 13 to 44 nm, which is comparable with previously reported experimental results (36) and MD prediction (37). As expected, the slip velocity increases with increasing angular velocity because of the increase in the strain rate (the gradient of velocity field) (38). We also found that salt rejection increases with the increase in slip velocity (Fig. 2F), thus motivating us to investigate potential connections between boundary slip and ion selectivity.

To identify whether the high salt rejection is solely attributed to the slip velocity at the water-graphene interface, we construct another shearing membrane model using a flat monolayer graphene without centrifugal force to separate the effect of boundary slip from centrifugal force. As shown in Fig. 3A, a 7.1 nm-by-7.2 nm monolayer graphene of a single pore with 2 nm in diameter (porosity of 6.14%) is located at 7 nm in z direction, and the shearing motion is prescribed in $-x$ direction as the velocity varies in the range of 0 to 350 m/s (see movie S2 for the graphene velocity of 25 m/s). The MD simulation details can be found in section S7. Intriguingly, the slip velocity across the graphene surface effectively improves the salt

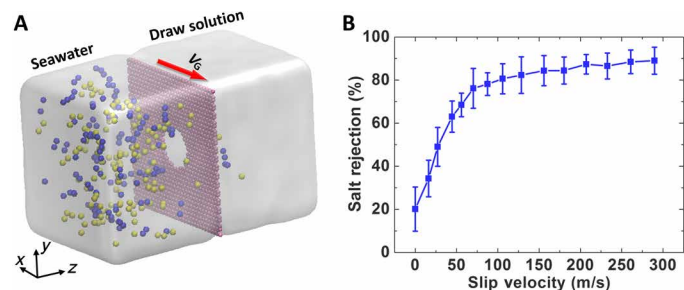


Fig. 3. Ultrahigh salt rejection induced by slip velocity in the model of shearing pored graphene. (A) Schematic illustration of shearing pored graphene model. Seawater including sodium ions (blue), chloride ions (yellow), and transparent water molecules is confined in the left region, and pure water is confined in the right region. The monolayer graphene, with a 2-nm-diameter pore located at the middle of the system, is moving at a constant velocity V_G (0 to 350 m/s) in $-x$ direction. The pored graphene is located at 7.0 nm in z direction, and the nanopore is located at (0,0) in $x-y$ plane initially. (B) Salt rejection as a function of the slip velocity at feed seawater-graphene interface for different shearing velocity.

rejection (Fig. 3B), while the water permeability remains as high as 101.43 ± 8 liter/cm² per day per MPa. From Fig. 3B, another exceptional finding is that the varying trend of the salt rejection versus slip velocity is consistent with that in Fig. 2F for the rotating porous GC of 12 pores. Therefore, we conclude that the interfacial slip between water and the porous graphene membrane results in an ultrahigh salt rejection even with large pores that are much bigger than the hydrated ions.

To reveal the underlying mechanism of slip-induced salt rejection, we plot the schematic illustration and trajectories of a blocked

sodium ion and a penetrated water molecule in Fig. 4. Figure 4A schematically shows a hydrated ion bounced off the pore edge (also see movie S3), while a water molecule was able to pass through the pore. With a shear velocity of 350 m/s (see movie S4), a single pore passes through the simulation domain periodically in x direction 25 times during the total simulation time of 0.5 ns, i.e., each ion/molecule that is close to the membrane and in the pore region (the green regions in Fig. 4, B and C) has 25 chances to pass through the pore. However, both hydrated sodium and chloride ions around the pore bounce off the pore edge repeatedly. As shown in Fig. 4B, there are four trajectory peaks for a blocked sodium ion extremely close to the graphene membrane at the pore region during 0.05 to 0.16 ns. In comparison, water molecules are able to pass through the pore without any bouncing-off events (see Fig. 4C). We also observe that a chloride ion was bounced back multiple times before it lastly seized an opportunity to permeate through the pore to the other side of GC (0.06 to 0.34 ns; see fig. S6). These results indicate that the large ratio of the tangential slip velocity across the graphene surface to the normal penetrating velocity can enable a high selectivity.

For the particles in the boundary layer near GC with negligible radial velocities, the only way they can exit from GC is when they come close to the opening of nanopores. Theoretically, each hydrated ion around the pore at the boundary of feed solution experiences a force of $F_i = P_f A_i$ approximately, where P_f is the internal pressure within the feed solution and $A_i = \frac{\pi d_i^2}{4}$ (d_i is the diameter of a hydrated ion) is the effective section area of a hydrated ion. Neverthe-

less, if the hydrated ions are not perfectly aligned with the pore opening when they first arrive at the graphene surface from radial direction, it requires a finite screen time for them to pass through the pore when they move to the pore opening from the circumference or longitudinal directions on the GC surface. This screen time can be calculated as follows: First, we can calculate the radial acceleration of the ion by Newton's second law, $a_i = \frac{F_i}{m_i} = \frac{P_f \pi d_i^2}{4 m_i}$, where m_i is the mass of a hydrated ion. Hence, the penetration distance of a particle can be found from the equation of motion: $\delta_p = \frac{1}{2} a_i t_p^2$, where δ_p is the effective thickness of the graphene membrane in radial direction, and t_p is the penetration time, which is the time needed for a hydrated ion to permeate through the pore. One can see that the larger mass of hydrated ion m_i leads to a smaller acceleration and hence longer penetration time. Another key parameter is t_c , the time needed for a hydrated ion tangentially moving across the pore on GC surface in tangential direction without penetrating the pore, $t_c = d/v_s$, where d is the pore diameter and v_s is the surface slip velocity. Therefore, if t_c is less than t_p ($t_c < t_p$), then a hydrated ion will not be able to pass through the porous graphene membrane even for the relative size of the hydrated ion and the pore $\alpha = d/d_i > 1$. It thus provides a novel separation mechanism based on time dimension. Similarly, when $t_c < t_p$ for water molecules, the water flux for GC rotating at an ultrahigh angular velocity, which can be demonstrated by the results of Fig. 2D (also in figs. S2C, S3C, and S4C). Then, a constraint condition for pore diameter d can be obtained as $v_s \cdot \sqrt{\frac{8\delta_p m_w}{P_f \pi}} < d^2 < \alpha v_s \cdot \sqrt{\frac{8\delta_p m_i}{P_f \pi}}$ (where m_w is the mass of a water molecule) to achieve an almost perfect desalination (see section S8). By carefully choosing parameters v_s , m , and δ_p , one can design a porous membrane with super large pore size, as long as P_f exceeds the osmosis pressure, and $\alpha > 1$.

Because the slip-induced salt rejection is intrinsically relying on the penetration time difference caused by mass difference in the time dimension, we thus propose a novel separation mechanism coined as the "temporal selectivity" or the fourth dimensional selectivity. Obviously, the pore size for the temporal selectivity explicitly depends on the slip velocity at the boundary of feed solution, the thickness of membrane, and the mass of solute particles for the same driving pressure.

To sum up, we have discovered that the nanoporous membrane with super large pore size can still realize high-efficiency desalination if ions have large boundary slip at the interface between feed solution and membrane. By increasing the relatively thicker membrane and larger mass of ions, one may attain the temporal selectivity for the membranes with even larger pore (>4 nm). Currently, the desalination principle of all the static porous RO membranes generally relies on the spatial three-dimensional selectivity based on the size difference between solute and solvent particles in the spatial dimension. The selectivity in time dimension can effectively bypass the limitation of the pore size to obtain an ultrahigh water permeability and will further reduce the requirements in fabricating uniformly sized small nanopores on RO membranes.

In porous membrane desalination devices, water flux is approximately proportional to the product of surface porosity ϵ by the squared pore radius r_p (2, 29). To study the influences of porosity and pore size on the performances of rotating porous membranes, we plot both the water flux and salt rejection as functions of the porosity of a rotating GCs of 12 to 72 pores in Fig. 5A. The water flux

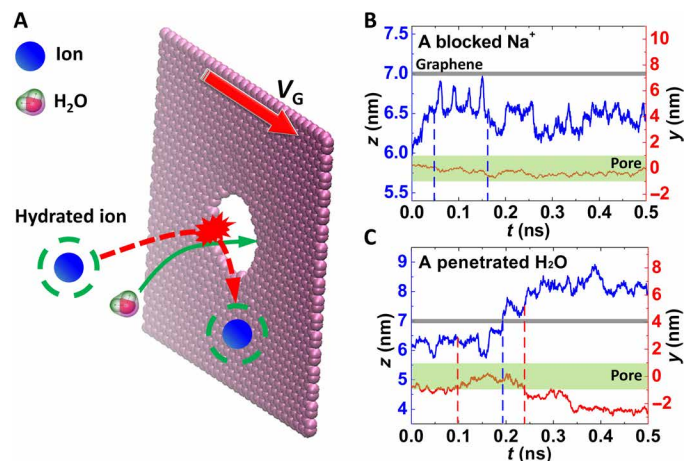


Fig. 4. Trajectory analysis of slip-induced salt rejection. (A) Schematic illustration of trajectories for both a hydrated ion and a penetrated water molecule to explain the mechanism of the slip-induced selectivity. The red dashed line is the trajectory of a block hydrated ion blocked by the pore edge. The green solid line is the trajectory of a water molecule passing through the pore, and the green dashed circles denote the hydration shell around the ion. (B) and (C) plot the trajectories in y (blue) and z (red) directions for a blocked sodium and a penetrated water molecule, respectively. The dark gray lines denote the pored graphene locating at 7 nm in z direction, and the transparent green region corresponds to the pored region in y direction. The section confined two dashed blue lines in subfigure (B) means that the sodium ion close to the pore is bounced back four times during this period. In subfigure (C), the section between two red dashed lines means that the water molecule is locating at the pore region, and the dashed blue lines denote that the water molecule passes through the pore at $t = 0.19$ ns.

increases, but salt rejection decreases with the increase in porosity. Then, we consider the effect of porosity on the boundary slip velocity at the feed-membrane interface in the proposed temporal selectivity model, as shown in Fig. 5B. The related velocity profiles and the results of slip versus porosity for different rotating angular velocities can be found in section S9 (fig. S7, A and B). Obviously, the increase in porosity significantly reduces the slip velocity due to the increase in the feed-membrane interfacial friction (39). Inherently, the increase in the number of pores, which is equivalent of more defects on the membranes, enhances the roughness of the porous graphene. Subsequently, the salt rejection versus the slip velocity for different porosities is plotted in Fig. 5C. It can be observed that the salt rejection is almost independent of porosity, which is consistent with the conventional RO membranes. In particular, if we further enlarge the pore size to 3 or 4 nm in diameter while keeping the porosity constant, the salt rejection can also be improved significantly if a large enough slip velocity is provided at the feed-membrane interface (see Fig. 5D). Moreover, the salt rejection decreases with enlarged pore size, and meanwhile, the water flux is also reduced at a high angular velocity because more penetrating ions occupy the porous channels (see section S9: fig. S7, C and D). Thus, as for the slip-induced salt rejection, the pore size is also a key optimization parameter to determine the upper bound of permeability-selectivity trade-off.

DISCUSSION

In Fig. 6, we compared the permeability and selectivity of the rotating porous GC with those of the reported representative membranes including commercial TFC RO membranes (29), nanoporous graphene membranes (4, 9, 11), GO frameworks (40), graphene-CNT (GCNT) hybrid membrane (30), MoS₂ membranes (25), CNTs with various sizes (13), and covalent triazine frameworks (CTFs) (41).

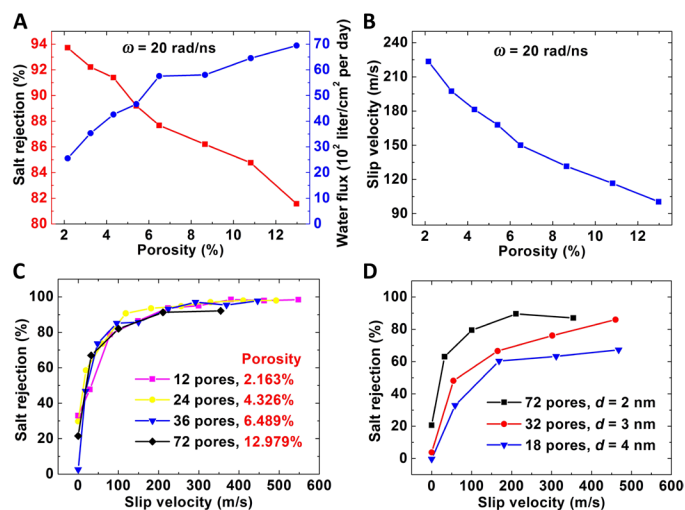


Fig. 5. Influences of porosity and pore size on permeability and selectivity. (A) Porosity dependence on both salt rejection and water flux. (B) Slip velocity as a function of porosity for the angular velocity of 20 rad/ns. The porosity of the rotating GC changes from 2.163% (12 pores) to 12.979% (72 pores). (C) Salt rejection versus slip velocity for different porosities. (D) Salt rejection versus slip velocity for different pore diameters in the range of 2 to 4 nm, while the porosity is kept as a constant of 12.979%.

The membranes with enhanced ion selectivity have been realized in many previous experimental and modeling studies (4, 9, 11, 40) even including commercial RO membranes (29). At present, researches on developing novel membranes have mostly focused on improving water permeability rather than on ion selectivity (24). Figure 6 displays some optimum data of salt rejection versus permeability for different angular velocities, porosities of GCs with 2-nm pores, which were obtained in this work. It can be seen that the water permeability of the rotating porous graphene increases up to 101 to 176 liter/cm² per day per MPa for the salt rejection above 95%, which is 350 to 1000 times larger than the reported best commercial membranes (29) and several times larger than the reported largest water permeability of 66 liter/cm² per day per MPa for porous graphene membranes (4) and 64.2 liter/cm² per day per MPa for CTFs (41). Compared with the most recent experimental results, e.g., (30), the water permeability in this work can be more than three times larger than that of GCNT hybrid membrane for the same salt rejection of 86% (see section S10: fig. S8). In particular, both the required water permeability and salt rejection can be obtained easily by adjusting the angular velocity for different porosities and pore sizes. Although the proposed rotating porous GC model will face challenges for scaling up to practical membrane sizes on the meter scale (42), excitingly, nanometer-sized pores have been created experimentally in a monolayer graphene using an oxygen plasma etching process (9), which provides the possibility to scale up the porous graphene-based centrifuge for water purification and desalination. The feasibility analysis and design of a scale-up porous graphene centrifuge can be found in section S11.

To further prove the concept of the proposed temporal selectivity, we investigate the influences of divalent ions and salt concentration in feed solution on desalination performances, which is discussed in

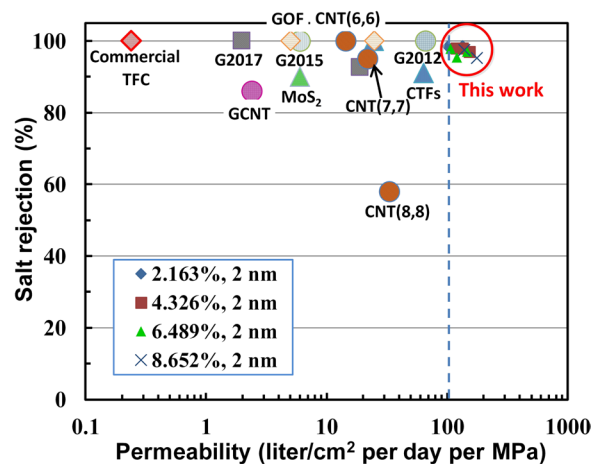


Fig. 6. Comparison of permeability and salt rejection with other state-of-the-art RO membranes. Detailed comparisons of permeability and salt rejection of the rotating porous graphene membrane with other membranes, including commercial TFC RO membranes, nanoporous graphene membranes (G2012, G2015, and G2017), graphene oxide frameworks (GOF), graphene-CNT (GCNT) hybrid membrane, MoS₂ membranes, various sized CNTs, covalent triazine frameworks (CTFs) and some optimum results (salt rejection larger than 95%) of GCs with 2 nm pores in this work (in red circle). The optimum data in this work are illustrated in label list for different angular velocities (30 to 40 rad/ns) and porosities (2.163% to 8.652%). The data in other works are labeled individually in brief.

section S12. As expected, the divalent Ca^{2+} ions with higher mass and larger hydrated radius can hardly pass through the rotating porous GC, whereas the amount of chloride ions in CaCl_2 feed solution that can pass through GC is almost equal to that in NaCl feed solution (fig. S10, A and B). This is because the higher mass of Ca^{2+} results in lower acceleration in penetrating direction, thereby leads to a longer penetrated time t_p for the same membrane thickness, making it more difficult for them to penetrate the porous GC (fig. S10, C and D). In addition, a decrease in salt concentration increases the slip velocity at the boundary of feed solution (fig. S10, E to H) and decreases the time needed for a hydrated ion tangentially moving across the pore (t_c), thus resulting in an increase in salt rejection. All these results can be clearly explained by temporal selectivity.

Moreover, the typical pore edges of graphene membrane are usually decorated by hydrogen or hydroxyl groups (4). As for the shearing-induced desalination based on the single pored graphene model (see section S13), the results indicate that the chemical groups added on the pore edge decreases the slip velocity at the feed solution-graphene interface, because the charged chemical groups increase the coupling strength at the solid-liquid interface and further increase the interfacial friction. According to the proposed temporal selectivity, the reduced slip velocity may decrease the salt rejection and increase the water permeability for the same pore size. However, this effect needs to be further investigated in the future work.

It should be noted that as mentioned above, in some cases, we may achieve almost 100% salt rejection but never a complete 100% salt rejection. This is because that there will be small percentage hydrated ions that are arriving at the boundary of the porous membrane perfectly aligned with the pore opening location with significant radial velocities, and thus, they can follow their initial trajectories easily exiting the porous membrane without delay. This is the reason why we cannot achieve a complete 100% salt rejection. Moreover, as the porosity increases, the chance that a particle having a direct hit with the opening of a pore will increase. Because the proposed temporal selection principle does not apply to the hydrated ions with the direct hit with pores, the salt rejection must decline as the porosity of GC increases.

Hydrophobic nature of graphene membrane will significantly reduce the boundary friction between feed solution and GC, resulting in super large surface sliding velocities for hydrated sodium and chloride ions (12). Because of such large surface sliding velocities of the hydrated ions, in this work, we found that the rotating nanoporous monolayer GC with large pores (2 to 4 nm) is still able to achieve ultrahigh water permeability and salt rejection simultaneously, breaking the permeability-selectivity paradox or trade-off in the membrane separation-based RO process. The unprecedented water permeability may make the rotating membranes highly attractive for RO energy-efficient desalination and water purification. An intriguing mechanism of the salt rejection caused by the large surface slip velocity at the feed solution-GC interface is discovered and revealed, and meanwhile, the large nanopores collaborating with the centrifugal pressure provide an ultrahigh water permeability. This discovery promotes a new concept of the temporal selectivity or the fourth dimensional selectivity, because the slip-induced salt rejection is relying on the penetration time difference between hydrated ions and water molecules caused by mass difference in temporal dimension. The salt rejection can also be improved significantly even if the pore size is enlarged to 3 to 4 nm in diameter. Moreover, the desired water permeability and selectivity can be conve-

niently obtained by adjusting the rotating angular velocity, the thickness of the membrane shell, and porosity and pore size of the membrane. Although the fabrication of a scale-up of the rotating membranes with large surface slip is still a work in progress, the exciting discovery on the novel membrane desalination mechanism and the rigorous results of MD simulation provide a solid chemical physics foundation and profound engineering inspirations for the design of large nanopore membranes with surface slip-induced ultrahigh selectivity and permeability.

MATERIALS AND METHODS

Molecular simulation method has been demonstrated to be a very effective tool to study the permeation processes of the graphene-based membranes involving the molecular transport in the confined space at nanoscale (43). In this study, a large-scale MD bench model consisting of a porous GC with 41.4 nm in diameter and 13.45 nm in length, 1,015,420 water molecules, 16,358 salt ions (8179 Na^+ and 8179 Cl^- , respectively), and two pored graphene sheets to confine draw solution is constructed to study the related seawater desalination processes, which is schematically shown in Fig. 1. The size of the simulation box in x - y - z dimensions is 45.5 nm by 45.5 nm by 15.8 nm with the axis of porous GC locating at the center of x - y plane. The nanopores of 2 to 4 nm in diameter are created by directly removing the corresponding carbon atoms on GC without passivating the pore edges with functional groups, because the edge effect of nanopores can be ignored when the pore size is two to five times larger in diameter than hydrated sodium ions. The initial salinity of the seawater confined in GC is $\sim 3.5\%$, which is the mean salinity of the world's oceans. The initial pressure within feed solution for the membrane without rotation is 6 MPa, which is larger than the osmotic pressure of 2.78 MPa approximately derived from thermodynamics (44). The rotating angular velocity of GC is in the range of 0 to 40 rad/ns. Periodic boundary conditions are used in all three dimensions of simulation box. The details of MD simulation and corresponding parameters can be found in section S1. The movie of a representative graphene centrifuge with 36 pores rotating at an angular velocity of 35 rad/ns is provided in movie S1.

SUPPLEMENTARY MATERIALS

Supplementary material for this article is available at <http://advances.sciencemag.org/cgi/content/full/6/34/eaba9471/DC1>

REFERENCES AND NOTES

1. M. Elimelech, W. A. Phillip, The future of seawater desalination: Energy, technology, and the environment. *Science* **333**, 712–717 (2011).
2. A. Boretti, S. Al-Zubaidy, M. Vaclavikova, M. Al-Abri, S. Castelletto, S. Mikhailovsky, Outlook for graphene-based desalination membranes. *NPJ Clean Water* **1**, 5 (2018).
3. G. P. Liu, W. Q. Jin, N. P. Xu, Graphene-based membranes. *Chem. Soc. Rev.* **44**, 5016–5030 (2015).
4. D. Cohen-Tanugi, J. C. Grossman, Water desalination across nanoporous graphene. *Nano Lett.* **12**, 3602–3608 (2012).
5. E. N. Wang, R. Karnik, Water desalination: Graphene cleans up water. *Nat. Nanotechnol.* **7**, 552–554 (2012).
6. S. P. Koenig, L. D. Wang, J. Pellegrino, J. S. Bunch, Selective molecular sieving through porous graphene. *Nat. Nanotechnol.* **7**, 728–732 (2012).
7. S. C. O'Hern, C. A. Stewart, M. S. H. Boutilier, J. C. Idrobo, S. Bhaviripudi, S. K. Das, J. Kong, T. Laoui, M. Atieh, R. Karnik, Selective molecular transport through intrinsic defects in a single layer of CVD graphene. *ACS Nano* **6**, 10130–10138 (2012).
8. S. C. O'Hern, M. S. H. Boutilier, J. C. Idrobo, Y. Song, J. Kong, T. Laoui, M. Atieh, R. Karnik, Selective ionic transport through tunable subnanometer pores in single-layer graphene membranes. *Nano Lett.* **14**, 1234–1241 (2014).

9. S. P. Surwade, S. N. Smirnov, I. V. Vlassioux, R. R. Unocic, G. M. Veith, S. Dai, S. M. Mahurin, Water desalination using nanoporous single-layer graphene. *Nat. Nanotechnol.* **10**, 459–464 (2015).
10. T. Jain, B. C. Raseria, R. J. S. Guerrero, M. S. H. Boutilier, S. C. O'Hern, J. C. Idrobo, R. Karnik, Heterogeneous sub-continuum ionic transport in statistically isolated graphene nanopores. *Nat. Nanotechnol.* **10**, 1053–1057 (2015).
11. Y. H. Wang, Z. J. He, K. M. Gupta, Q. Shi, R. F. Lu, Molecular dynamics study on water desalination through functionalized nanoporous graphene. *Carbon* **116**, 120–127 (2017).
12. G. Hummer, J. C. Rasaiah, J. P. Noworyta, Water conduction through the hydrophobic channel of a carbon nanotube. *Nature* **414**, 188–190 (2001).
13. B. Corry, Designing carbon nanotube membranes for efficient water desalination. *J. Phys. Chem. B* **112**, 1427–1434 (2008).
14. M. Majumder, N. Chopra, R. Andrews, B. J. Hinds, Nanoscale hydrodynamics - Enhanced flow in carbon nanotubes. *Nature* **438**, 44–44 (2005).
15. J. K. Holt, H. G. Park, Y. M. Wang, M. Stadermann, A. B. Artyukhin, C. P. Grigoropoulos, A. Noy, O. Bakajin, Fast mass transport through sub-2-nanometer carbon nanotubes. *Science* **312**, 1034–1037 (2006).
16. B. J. Hinds, N. Chopra, T. Rantell, R. Andrews, V. Gavalas, L. G. Bachas, Aligned multiwalled carbon nanotube membranes. *Science* **303**, 62–65 (2004).
17. M. Majumder, N. Chopra, B. J. Hinds, Effect of tip functionalization on transport through vertically oriented carbon nanotube membranes. *J. Am. Chem. Soc.* **127**, 9062–9070 (2005).
18. F. Fornasiero, H. G. Park, J. K. Holt, M. Stadermann, C. P. Grigoropoulos, A. Noy, O. Bakajin, Ion exclusion by sub-2-nm carbon nanotube pores. *Proc. Natl. Acad. Sci. U.S.A.* **105**, 17250–17255 (2008).
19. W.-F. Chan, H. Y. Chen, A. Surapathi, M. G. Taylor, X. H. Shao, E. Marand, J. K. Johnson, Zwitterion functionalized carbon nanotube/polyamide nanocomposite membranes for water desalination. *ACS Nano* **7**, 5308–5319 (2013).
20. R. R. Nair, H. A. Wu, P. N. Jayaram, I. V. Grigorieva, A. K. Geim, Unimpeded permeation of water through helium-leak-tight graphene-based membranes. *Science* **335**, 442–444 (2012).
21. H. W. Kim, H. W. Yoon, S. M. Yoon, B. M. Yoo, B. K. Ahn, Y. H. Cho, H. J. Shin, H. Yang, U. Paik, S. Kwon, J. Y. Choi, H. B. Park, Selective gas transport through few-layered graphene and graphene oxide membranes. *Science* **342**, 91–95 (2013).
22. H. Li, Z. N. Song, X. J. Zhang, Y. Huang, S. G. Li, Y. T. Mao, H. J. Ploehn, Y. Bao, M. Yu, Ultrathin, molecular-sieving graphene oxide membranes for selective hydrogen separation. *Science* **342**, 95–98 (2013).
23. R. K. Joshi, P. Carbone, F. C. Wang, V. G. Kravets, Y. Su, I. V. Grigorieva, H. A. Wu, A. K. Geim, R. R. Nair, Precise and ultrafast molecular sieving through graphene oxide membranes. *Science* **343**, 752–754 (2014).
24. J. Abraham, K. S. Vasu, C. D. Williams, K. Gopinadhan, Y. Su, C. T. Cheria, J. Dix, E. Prestat, S. J. Haigh, I. V. Grigorieva, P. Carbone, A. K. Geim, R. R. Nair, Tunable sieving of ions using graphene oxide membranes. *Nat. Nanotechnol.* **12**, 546–550 (2017).
25. Z. Y. Wang, Q. S. Tu, S. X. Zheng, J. J. Urban, S. F. Li, B. X. Mi, Understanding the aqueous stability and filtration capability of MoS₂ membranes. *Nano Lett.* **17**, 7289–7298 (2017).
26. Z. Y. Wang, B. X. Mi, Environmental applications of 2D molybdenum disulfide (MoS₂) nanosheets. *Environ. Sci. Technol.* **51**, 8229–8244 (2017).
27. S. Homaeigohar, M. Elbahri, Graphene membranes for water desalination. *NPG Asia Mater.* **9**, e427 (2017).
28. D. Cohen-Tanugi, J. C. Grossman, Nanoporous graphene as a reverse osmosis membrane: Recent insights from theory and simulation. *Desalination* **366**, 59–70 (2015).
29. J. R. Werber, C. O. Osuji, M. Elimelech, Materials for next-generation desalination and water purification membranes. *Nat. Rev. Mater.* **1**, 16018 (2016).
30. Y. B. Yang, X. D. Yang, L. Liang, Y. Y. Gao, H. Cheng, X. M. Li, M. C. Zou, A. Y. Cao, R. Z. Ma, Q. Yuan, X. F. Duan, Large-area graphene-nanomesh/carbon-nanotube hybrid membranes for ionic and molecular nanofiltration. *Science* **364**, 1057–1062 (2019).
31. C. T. Nguyen, A. Beskok, Charged nanoporous graphene membranes for water desalination. *Phys. Chem. Chem. Phys.* **21**, 9483–9494 (2019).
32. C. T. Nguyen, A. Beskok, Saltwater transport through pristine and positively charged graphene membranes. *J. Chem. Phys.* **149**, 024704 (2018).
33. Z. Q. Tian, S. M. Mahurin, S. Dai, D. E. Jiang, Ion-gated gas separation through porous graphene. *Nano Lett.* **17**, 1802–1807 (2017).
34. C. Z. Sun, S. H. Zhu, M. C. Liu, S. H. Shen, B. F. Bai, Selective molecular sieving through a large graphene nanopore with surface charges. *J. Phys. Chem. Lett.* **10**, 7188–7194 (2019).
35. M. Ma, G. Tocci, A. Michaelides, G. Aeppli, Fast diffusion of water nanodroplets on graphene. *Nat. Mater.* **15**, 66–71 (2016).
36. Q. Xie, M. A. Alibakhshi, S. P. Jiao, Z. P. Xu, M. Hempel, J. Kong, H. G. Park, C. H. Duan, Fast water transport in graphene nanofluidic channels. *Nat. Nanotechnol.* **13**, 238–245 (2018).
37. J. A. Thomas, A. J. H. McGaughey, Reassessing fast water transport through carbon nanotubes. *Nano Lett.* **8**, 2788–2793 (2008).
38. P. A. Thompson, S. M. Troian, A general boundary condition for liquid flow at solid surfaces. *Nature* **389**, 360–362 (1997).
39. K. Falk, F. Sedlmeier, L. Joly, R. R. Netz, L. Bocquet, Molecular origin of fast water transport in carbon nanotube membranes: superlubricity versus curvature dependent friction. *Nano Lett.* **10**, 4067–4073 (2010).
40. A. Nicolai, B. G. Sumpter, V. Meunier, Tunable water desalination across graphene oxide framework membranes. *Phys. Chem. Chem. Phys.* **16**, 8646–8654 (2014).
41. L. C. Lin, J. Choi, J. C. Grossman, Two-dimensional covalent triazine framework as an ultrathin-film nanoporous membrane for desalination. *Chem. Commun.* **51**, 14921–14924 (2015).
42. B. X. Mi, Scaling up nanoporous graphene membranes. *Science* **364**, 1033–1034 (2019).
43. C. Sun, M. Liu, B. Bai, Molecular simulations on graphene-based membranes. *Carbon* **153**, 481–494 (2019).
44. G. Scatchard, Physical chemistry of protein solutions. I. Derivation of the equations for the osmotic pressure. *J. Am. Chem. Soc.* **68**, 2315–2319 (1946).
45. D. W. Brenner, O. A. Shenderova, J. A. Harrison, S. J. Stuart, B. Ni, S. B. Sinnott, A second-generation reactive empirical bond order (REBO) potential energy expression for hydrocarbons. *J. Phys. Condens. Matter* **14**, 783–802 (2002).
46. K. H. Lee, P. Keblinski, S. B. Sinnott, Deflection of Nanotubes in Response to External Atomic Collisions. *Nano Lett.* **5**, 263–268 (2005).
47. R. Rafiee, R. M. Moghadam, On the modeling of carbon nanotubes: A critical review. *Compos. Part B Eng.* **56**, 435–449 (2014).
48. W. L. Jorgensen, J. Chandrasekhar, J. D. Madura, R. W. Impey, M. L. Klein, Comparison of simple potential functions for simulating liquid water. *J. Chem. Phys.* **79**, 926–935 (1983).
49. H. W. Horn, W. C. Swope, J. W. Pitera, J. D. Madura, T. J. Dick, G. Hura, T. Headgordon, Development of an improved four-site water model for biomolecular simulations: TIP4P-Ew. *J. Chem. Phys.* **120**, 9665–9678 (2004).
50. R. Qiao, N. R. Aluru, Atypical dependence of electroosmotic transport on surface charge in a single-wall carbon nanotube. *Nano Lett.* **3**, 1013–1017 (2003).
51. J. Delhomelle, P. Millié, Inadequacy of the Lorentz-Berthelot combining rules for accurate predictions of equilibrium properties by molecular simulation. *Mol. Phys.* **99**, 619–625 (2001).
52. S. Plimpton, Fast parallel algorithms for short-range molecular dynamics. *J. Comput. Phys.* **117**, 1–19 (1995).
53. X. Zhu, D. M. Villeneuve, A. Y. Naumov, S. Nikumb, P. B. Corkum, Experimental study of drilling sub-10 μm holes in thin metal foils with femtosecond laser pulses. *Appl. Surf. Sci.* **152**, 138–148 (1999).

Acknowledgments

Funding: This work was conducted and completed at the University of California, Berkeley. Z.Z. was supported by the National Natural Science Foundation of China (NSFC) with grants 11872192, 11772082, and 11672063. **Author contributions:** S.L. and Z.Z. conceived the idea and concept of the project. Z.Z. performed the simulations. All the authors analyzed the data and discussed the results. Z.Z. and S.L. wrote the paper. All authors edited and proofread the paper, made comments, and approved the manuscript. **Competing interests:** The authors declare that they have no competing interests. **Data and materials availability:** All data needed to evaluate the conclusions in the paper are present in the paper and/or the Supplementary Materials. Additional data related to this paper may be requested from the authors.

Submitted 17 January 2020

Accepted 8 July 2020

Published 19 August 2020

10.1126/sciadv.aba9471

Citation: Z. Zhang, S. Li, B. Mi, J. Wang, J. Ding, Surface slip on rotating graphene membrane enables the temporal selectivity that breaks the permeability-selectivity trade-off. *Sci. Adv.* **6**, eaba9471 (2020).

Surface slip on rotating graphene membrane enables the temporal selectivity that breaks the permeability-selectivity trade-off

Zhongqiang Zhang, Shaofan Li, Baoxia Mi, Jinbao Wang and Jianning Ding

Sci Adv 6 (34), eaba9471.
DOI: 10.1126/sciadv.aba9471

ARTICLE TOOLS

<http://advances.sciencemag.org/content/6/34/eaba9471>

SUPPLEMENTARY MATERIALS

<http://advances.sciencemag.org/content/suppl/2020/08/17/6.34.eaba9471.DC1>

REFERENCES

This article cites 53 articles, 10 of which you can access for free
<http://advances.sciencemag.org/content/6/34/eaba9471#BIBL>

PERMISSIONS

<http://www.sciencemag.org/help/reprints-and-permissions>

Use of this article is subject to the [Terms of Service](#)

Science Advances (ISSN 2375-2548) is published by the American Association for the Advancement of Science, 1200 New York Avenue NW, Washington, DC 20005. The title *Science Advances* is a registered trademark of AAAS.

Copyright © 2020 The Authors, some rights reserved; exclusive licensee American Association for the Advancement of Science. No claim to original U.S. Government Works. Distributed under a Creative Commons Attribution NonCommercial License 4.0 (CC BY-NC).